HHS Public Access

Author manuscript

Environ Res. Author manuscript; available in PMC 2017 July 24.

Published in final edited form as:

Environ Res. 2016 April ; 146: 173–184. doi:10.1016/j.envres.2015.12.027.

Validation of Research Trajectory 1 of an Exposome Framework: Exposure to benzo(a)pyrene confers enhanced susceptibility to bacterial infection

Ryan S. Clark[a], **Samuel T. Pellom**[b,c], **Burthia Booker**[b], **Aramandla Ramesh**[c], **Tongwen Zhang**[d], **Anil Shanker**[c], **Mark Maguire**[a], **Paul D. Juarez**[e], **Patricia Matthews-Juarez**[e], **Michael A. Langston**[f], **Maureen Y. Lichtveld**[g], and **Darryl B. Hood**[a,d]

[a]Department of Neuroscience and Pharmacology, Meharry Medical College, Nashville, TN 37208

[b]Department of Microbiology, Meharry Medical College, Nashville, TN 37208

[c]Department of Biochemistry and Cancer Biology, Meharry Medical College, Nashville, TN 37208

[d]Division of Environmental Health Sciences, College of Public Health, The Ohio State University, Columbus, OH 43210

[e]Department of Family and Preventive Medicine, Meharry Medical College, Nashville, TN 37208

[f]Department of Electrical Engineering and Computer Science, University of Tennessee, Knoxville, TN 37996

[g]Department of Global Environmental Health Sciences, School of Public Health & Tropical Medicine, Tulane University, 1440 Canal Street, New Orleans, LA 70112

Abstract

The exposome provides a framework for understanding elucidation of an uncharacterized molecular mechanism conferring enhanced susceptibility of macrophage membranes to bacterial infection after exposure to the environmental contaminant benzo(a)pyrene, [B(a)P]. The fundamental requirement in activation of macrophage effector functions is the binding of immunoglobulins to Fc receptors. FcγRIIa (CD32a), a member of the Fc family of immunoreceptors with low affinity for immunoglobulin G, has been reported to bind preferentially to IgG within lipid rafts. Previous research suggested that exposure to B(a)P suppressed macrophage effector functions but the molecular mechanisms remained elusive. The goal of this study was to elucidate the mechanism(s) of B(a)P-exposure induced suppression of macrophage function by examining the resultant effects of exposure-induced insult on CD32-lipid raft interactions in the regulation of IgG binding to CD32. The results demonstrate that exposure of

Corresponding author: Darryl B. Hood, Ph.D., Division of Environmental Health Sciences, College of Public Health; Department of Neuroscience, College of Medicine, The Ohio State University, Columbus, OH USA. Phone (614) 247-4941, FAX: (614) 292-4053, hood.188@osu.edu.

Conflicts of Interest: The authors declare no conflict of interest.

macrophages to B(a)P alters their lipid raft integrity by decreasing membrane cholesterol 25% while increasing CD32 into non-lipid raft fractions. This robust diminution in membrane cholesterol and 30% exclusion of CD32 from lipid rafts causes a significant reduction in CD32-mediated IgG binding to suppress essential macrophage effector functions. Such exposures across the lifespan would have the potential to induce an immunosuppressive endophenotypes in vulnerable populations.

Keywords

Benzo(a)pyrene; immune suppression; lipid rafts; membrane integrity; FcγRII (CD32) antibody

INTRODUCTION

Recently we proposed the Public Health Exposome (Juarez et al., 2014) as an opportunity for establishing a translational framework, applying transdisciplinary tools, and developing an evidence base for health disparities research, practice, policy, community engagement, and research training. At a recent meeting of the “Exposome” Symposium to Explore the Intersection of Environmental Exposure and Disease” at Duke University (April, 3, 2015), consensus emerged that there is a single exposome comprised of both internal and external environments, pathways, and mechanisms. This paper adheres to this new consensus.

The Exposome paradigm is grounded in systems theory (von Bertalanffy, 2003) and a life cycle approach (Bornstein, 1989). It provides a conceptual framework that can be used to identify and compare relationships between differential levels of exposure at critical life stages, personal health outcomes, and health disparities at a population level. The resulting relationships can be compared across space, place, and time. It allows for the generation and testing of hypotheses about exposure pathways and the mechanisms through which exogenous and endogenous exposures result in poor personal health outcomes and population level health disparities. An exposome approach enables the identification of at-risk persons and health populations experiencing disparate health outcomes. Ultimately, this approach will enable opportunities for enhancing genomic, clinical, and public health interpretations and interventions along an exposure pathway continuum.

Application of our concept by the exposure science community will promote advances in: 1) individual exposure characterization; 2) community-level, environmental, epidemiological cohort studies; 3) health disparities research; 4) community-based participatory research (CBPR) methods; 5) research at the intersection of the eco-system and human health; and 6) training of a new cadre of emerging transdisciplinary scholars. The full benefit of the Public Health Exposome framework will be realized when two environmental health research trajectory vectors converge at the level of population studies indicated by the upper right quadrant in Figure 1 (below). With this article we present our rationale for this trajectory, by means of an exemplar based on physiological dysregulation (e.g., immune response) representing knowledge gained (on a continuum) from basic science research.

Currently, there are significant resources being devoted to ascertaining the mechanism by which environmental contaminant exposure during the critical developmental windows

afford an enhanced susceptibility to bacterial infection in infants and young children. (Claude et al., 2012) It is well known that the PAH family of global environmental contaminants targets and suppresses virtually every component of cell-mediated and humoral immune response systems.(Braun et al., 1998; Li et al., 2002; Sarkar et al., 2012; Stevens et al., 2009; van Grevenynghe et al., 2003; Ramesh et al., 2011) The mechanism(s) by which PAH's modulate this apparent immunosuppression is poorly understood, and previous studies used animal models to evaluate possible mechanistic links. Data from animal studies suggest that AhR ligands such as B(a)P and 2, 3, 7, 8, tetrachloro, dibenzo-p-dioxin (TCDD) suppress immunity by their ability to compromise virtually every stage of lymphocyte development, activation, and effector function (Allan and Sherr, 2010; van Grevenynghe et al., 2005).

The plasma membrane constitutes the first cellular barrier encountered by xenobiotics. Xenobiotics such as B(a)P are usually both hydrophobic and lipophilic, which allows them to accumulate within the plasma membrane and exert an “analgesic” effect. Lipid rafts, also called detergent resistant membranes (DRMs), are unique plasma membrane compartments that are highly enriched in cholesterol, sphingolipids, and phospholipids containing saturated fatty acids. They play an important role in many cellular functions. A wide array of receptors constitutively reside within or associate with lipid rafts. These receptors bind to antibodies to induce signaling events that regulate many cell responses. Previous studies suggest that this binding activity depends on intact lipid rafts (Simons and Toomre, 2000). One family of immunoreceptors, the Fcγ receptors (FcγR), constitutively reside within lipid rafts where they bind to IgG molecules, and initiate signaling events that regulate defense responses (Beekman et al., 2008).

Fcγ receptors are widely expressed throughout the hematopoietic system. Innate immune effector cells, such as monocytes, macrophages, dendritic cells and basophils, express activating and inhibitory FcγRs (Nimmerjahn and Ravetch, 2008). Traditionally, FcγR families are categorized according to the receptor's affinity for specific IgG subclasses and the signaling pathway they trigger. Human FcyRIIA (CD32) is a receptor with a low to medium affinity for IgG molecules and is one of two FcγRs that can transduce activating signaling pathways autonomously (Ravetch and Bolland, 2001). Bearing an immunoreceptor tyrosine based activating motif (ITAM) on its cytoplasmic domain, the ITAM confers on CD32 the ability to initiate signaling events that regulate cellular responses including phagocytosis, respiratory burst and cytokine production.

Macrophages are cells of the innate immune system that constitute the first line of defense against many infectious diseases. Mature macrophages function in promoting the clearance of invading microorganisms by respiratory burst activity, phagocytosis, then excretion. It has been previously demonstrated in macrophages that CD32a-lipid raft interactions are essential for efficient signaling events and that toxicants such as MβCD (depletes membrane cholesterol), nystatin (binds cholesterol) and C3 and C6 ceramides disrupt binding by altering lipid raft integrity (Bournazos et al., 2009). To date there is some evidence for PAH exposure-induced suppression of both monocyte differentiation into macrophages and/or dendritic cells (Laupeze et al., 2002) as well as effector functions (Braun et al., 1998). However, the molecular level mechanism for this suppression remains elusive.

B(a)P is the archetypical member in the family PAHs. We hypothesized that the mechanism for B(a)P exposure-induced suppression of macrophage effector functions occur via disruption of lipid raft architecture thereby causing a decrease in CD32a within lipid rafts. To investigate this hypothesis as shown in Fig. 2A, we determined the cellular location of CD32a in the presence and absence of IgG, and examined the effect of B(a)P, MβCD, and nystatin on CD32a-IgG binding. Fig. 2B depicts our immunotoxicological interrogation of the effects of B(a)P exposure on lipid raft cholesterol concentration and the resulting accumulation of B(a)P metabolites within lipid rafts. The results demonstrate that in the absence of IgG, CD32a is mostly found outside lipid rafts and subsequently translocates to lipid rafts in the presence of IgG (Fig. 2A). As indicated in Fig. 2B, our results suggest that exposure to B(a)P significantly suppresses CD32a association with lipid rafts as compared to controls, leading to reduced IgGCD32a binding. Collectively, these findings suggest that intact lipid rafts are paramount for IgGCD32a binding and effector function signaling. These findings also support a role for B(a)P exposure in developmental immunotoxicity in that these exposures have the capacity to result in suppression of macrophage effector function by disrupting lipid raft integrity resulting in reduced IgG-CD32a binding and exposure-induced immunosuppressive endophenotypes leading to disparate health outcomes observed in vulnerable populations.

2. MATERIALS AND METHODS

2.1 Chemicals and Reagents

PE anti-human CD32 antibody, the mouse IgG2b isotype control, Human M-CSF, CD68-FITC, and the CD86-Alexa-Fluor antibodies were purchased from BioLegend (San Diego, CA). Benzo(a)pyrene [B(a)P] powder, Trypan blue, dimethyl sulfoxide (DMSO), dihydrorhodamine 123, and protease/phosphatase inhibitors were obtained from Sigma-Aldrich (St. Louis, MO). FITC-Dextran (M_r, 40,000 kDa) was purchased from Molecular Probes/Invitrogen (Carlsbad, CA). Phorbol 12-myristate 13-acetate (PMA) and Cholera Toxin Subunit B Hrp-conjugated ab (CTβ) were purchased from Abcam Biochemicals (Cambridge, MA). Specific antibodies to CD11b-PE, CD14-FITC, CD64, CD71-FITC, control IG1K and FITC were purchased from eBioscience (San Diego, CA). CD45 and CD59 were purchased from Santa Cruz Biotechnology (Dallas, TX). Amplex Red Cholesterol Assays and Anti-Human IgG(γ)-FITC conjugate ab were obtained from Invitrogen (Carlsbad, CA). Human IgG complexes (human heat-aggregated IgG; hHAIgG) were formed by incubating monomeric human IgG for 20 min at 63°C and centrifuged at 14,000 × g to removed precipitates.

2.2 Cultures of human CD14+ monocytes and generation of monocyte derived macrophages

Fresh human CD14+ monocytes were obtained from AllCells (Alameda, CA) and were cultured in RPMI 1640 medium supplemented with 10% heat-inactivated FBS (HyClone), 100U/ penicillin, 100 U/mL streptomycin (GIBCO) in the presence of DMSO, B(a)P (1,5, 10μM) or MCSF (50U/mL) for 6 days to differentiate monocytes derived macrophages as previously reported by (van Grevenynghe et al., 2003). Every three days the cells were harvested and provided fresh media with M-CSF and/or B(a)P. Cell viability, morphological

and phenotypic analysis were employed to identify macrophages. The cells were maintained at 37°C in a 95% air and 5% CO_2 incubator.

2.3 Trypan Blue Exclusion Assay for cell viability

For Trypan Blue staining, 100 μL of monocytic cells were incubated for 5 min with an equal volume of 0.4% (w/v) Trypan Blue solution prepared in deionized water. Cells were then counted in a dual chambered hemacytometer on a light microscope. Viable and non-viable cell counts were used to calculate percent viability. The cell viability for all experiments was 95% or better.

2.4 Flow Cytometry Staining and Analysis

FACS analysis of the cell surface expression of monocyte and macrophage phenotypic exposome markers CD11b, CD32, CD64, CD68, CD71, and CD86 was performed in both untreated and B(a)P treated monocyte cells. For this analysis monocytes were either untreated or treated with B(a)P and/or M-CSF, for up to 6 days in RPMI 1640 supplemented with 5 % FBS. As a positive control for differentiation, monocytes were treated with M-CSF (50 U/mL) for 6 days under same conditions. The cells were then transferred to 96-well, round bottom plates. The cells were pelleted, washed in PBS flow buffer (PBS+FBS), and labeled with conjugated antibodies at optimal concentrations (determined by prior studies) for 30 min on ice. The cells were washed twice with 200 μL of PBS flow buffer and fixed with 2% paraformaldehyde. Fixed cells were stored in the dark at 4°C, acquired, and analyzed within 3 days. Fifty-thousand events were acquired for each sample with a Guava EasyCyte Flow Cytometer (Millipore) and analyzed by FlowJo 10 software. Populations of monocytic cells were gated, as described previously (Thurmond and Gasiewicz, 2000). Immune complex binding was assessed based on a previously described assay (Hart et al., 2004) that measures binding of aggregated IgG to CD32, a low-affinity receptor via multiple binding sites that generate high-avidity interactions. Cells were incubated with human heat aggregate IgG complexes (hHAIgG) for 45 min on ice. The binding kinetics of IgG-CD32 was also measured following MβCD treatment (20mM). Cells were incubated with the corresponding hHAIgG for 45 min on ice. Cells were resuspended in 200 μL of wash buffer and fixed with 2% paraformaldehyde.

2.5 Phagocytosis determination assay

In order to assess the effects of B(a)P exposure of monocyte phagocytic functions, cells were cultured in complete RPMI 1640 supplemented with or without B(a)P (1, 5 or 10μM) and M-CSF (50 U/mL) for 6 days. After 6 days the cells were washed, incubated with 1 mg/mL FITC-dextran for 1 hr at 37°C. Cellular uptake of FITC-dextran was monitored by flow cytometry. A negative control was performed in parallel by incubating cells with FITC-dextran at 4°C. Flow cytometric data was analyzed as indicated above. Data is expressed as mean fluorescent intensity. Phagocytic Uptake profiles for Staphylococcus aureus and Escherichia coli uptake was determined by plating 1×10^4 monocytic cells on 35mm MatTek dishes in the absence or presence of M-CSF and/or B(a)P for 6 days. Cells were washed with cold PBS then incubated with CD68, and 50 mg/mL of S. aureus or E. coli bioparticles FITC-conjugate for 30 min. Phagocytosis was recorded on a Nikon confocal

microscope using Nikon imaging software elements advanced research. Twenty cells (ROIs) were selected and the intensity profile for each of the selected cells was analyzed.

2.6 Respiratory burst activity detection

. Respiratory burst activity detection was performed using the reactive oxygen intermediate-sensitive probe dihydrorhodamine 123. For this assay, CD14+ monocytes were either untreated or treated with B(a)P (1, 5 or 10μg) and/or M-CSF (50 U/mL) for 6 days in complete RPMI medium. Monocytes treated with M-CSF (50 U/mL) in complete RPMI served as positive control for differentiation. After incubation, cells were pelleted, washed and pre-stimulated for 30 min with 100 ng/mL PMA to trigger oxidative burst. After washing, cells were incubated with 5 μg/mL dihydrorhodamine 123 for 45 min at 37°C. Rhodamine 123 fluorescence in intact cells, formed by the action of reactive oxygen intermediates such as hydrogen peroxide, was then measured by flow cytometry. Data were expressed as fluorescence arbitrary units, or percentage fluorescent cells, as appropriate for comparison.

2.7 DRM fractionation and Dot blot analysis

DRM domain fractionation was performed as previously described (Popik and Alce, 2004) using well-validated protocols and all procedures were conducted at 4°C. Following stimulation of cells (1 × 10) with IgG complexes (hHAIgG), cells were washed with ice-cold PBS, incubated for 10 min with TNE buffer (50 mM Tris, 150 mM NaCl, and 2 mM EDTA (pH 7.5) at 4°C. A cocktail of protease and phosphatase inhibitors were added to the TNE buffer to inhibit endogenous protease and phosphatase activity. Cells were then homogenized and cell homogenates were incubated on ice for an additional 5 min, before the addition of Triton X-100 (0.25% v/v final concentration). Lysates were incubated for 30 min on ice and the supernatant (500 μl) was added to 500 μl of 80% sucrose density gradient medium was applied to the bottom of pre-chilled 14 mL ultracentrifuge tubes (Ultra-Clear; Beckman Coulter). On top, sucrose solutions at concentrations of 38% and 5% were sequentially layered. Samples were centrifuged at 36,000 × g for 18 hr at 4°C in an ultracentrifuge using a SW-41 rotor (Beckman Coulter). After centrifugation, nine (1mL) fractions were collected. Dot immunoassays were performed as described previously (Nguyen and Hildreth, 2000) Briefly, 200 μl portions of each fraction diluted 1 to 10 in PBS (2×10^5 cell equivalents) were added to wells of a Bio-Dot apparatus (Bio-Rad, Hercules, Calif.), gently suctioned onto nitrocellulose membranes, and allowed to air dry. These membranes were cut into strips and stored at −20°C in plastic bags. Before blotting, strips were blocked with 5% nonfat milk powder in TBST (10 mM Tris-HCl, pH 7.5; 100 mM NaCl; 0.1% Tween 20) for 1 hr at room temperature. Strips were then incubated with CD59 (a raft protein), CD45 (a non-raft protein) or CD32 antibody in TBST–0.5% milk powder for 2 hr and washed 10 min three times with TBST, followed by incubation with LI-COR (Lincoln, Nebraska) goat anti-human secondary Ab (1:1000) for 2 hr. The strips were then washed five times, visualized via LI-COR visualization system and band intensity was quantified using Image J (NIH) analyzed the bands.

2.8 Extraction, identification and quantitation of benzo(a)pyrene metabolites

Following the collection of fractions from the discontinuous sucrose density gradient, the samples were prepared by the technique as detailed in Myers et al. (2011). Lysed cell samples from control, M-CSF and B(a)P + M-CSF-exposed regimes were processed for analysis of B(a)P metabolites by liquid–liquid extraction and reverse phase high-performance liquid chromatography methods as described previously in Myers et al. (2011).

2.9 Liquid-liquid extraction (LLE)

500μL from each of the nine (1mL) sucrose gradient fractions were transferred to a 10 mL Corning screw cap tube. A volume of 1 mL HPLC grade water was added, followed by 3 mL of methanol and 1.5 mL of chloroform. The tubes were stirred vortexed for 60 sec and then centrifuged at 5,000 × g for 20 min. After centrifugation, the organic and aqueous layers were separated. The organic layer was carefully retrieved into another tube. The tube with the aqueous layer was subjected to a second extraction with water, methanol and chloroform as mentioned above. The organic layer was retrieved again. Organic phases from both extractions were combined and dried under a steady stream of nitrogen N_2. The residue was reconstituted in 300 μL of methanol, passed through Acrodisc filters (0.45 μm; 25 mm diameter; Gelman Sciences, Ann Arbor, MI) to remove particulates. A volume of 30 μL was injected onto HPLC. The lyophilized culture medium was reconstituted in 1 mL of sucrose-TKM buffer, subjected to LLE as mentioned above. After extraction, the samples were prepared for HPLC analysis.

2.10 HPLC analysis

B(a)P and its metabolites from the sucrose gradient fractions were resolved by a HPLC Model 1200 (Agilent Technologies, Wilmington, DE) equipped with a UV and fluorescence detector. The chromatograph was operated through a ChemStation (Agilent Technologies) for instrument control, data acquisition and analyses. 50 μL of samples were injected onto a C_{18} reverse phase column (ODS Pinnacle II, PAH column 4 μm, 250 × 2.1 mm; Restek Corporation, Bellefonte, PA). The column (temperature 33°C) was eluted for 45 min at a flow-rate of 1 mL/min with a ternary gradient of water: methanol: ethanol (40: 40: 20%) for 20 min, followed by the same gradient at a ratio of 30: 46: 24 for 10 min, 100% methanol for 10 min and returning to the initial gradient of 40:40:20 for 5 min. The excitation and emission wavelengths for the detector were 244 and 410 nm respectively. Benzo(a)pyrene metabolite standards were purchased from the National Cancer Institute Chemical Carcinogen Repository (Midwest Research Institute, Kansas City, MO). As B(a)P and its metabolite standards are potential carcinogens/mutagens, they were handled in accordance with NIH guidelines (NIH, 1981). Identification of the metabolites was accomplished by comparing retention times and peak areas of the samples with that of standards.

2.11 Confocal immunofluorescence microscopy

CD32 and Ctxβ immunolabeling was performed using previously described protocols. Briefly, monocytes were grown on sterile glass coverslips for 6 days (37°C; 5% CO_2) before immunolabeling. Cells were washed twice with ice-cold PBS and incubated with hrp-conjugated AF555 Ctxβ (1:1000) and CD32-PE Ab (1:1000) and for 45 min. The cells were

then washed three times with ice-cold PBS and fixed with 3.7% PFA for 15 min. To prevent endocytosis and ensure the plasma membranes of the cells were stained, all Ctxβ staining was performed on ice. The specificity of CtxB for the GM1 ganglioside was validated by dot blot analysis of monocyte cell lysates. Cells were then washed with ice-cold PBS and incubated with anti-human IgG-FITC for 30 min. Coverslips were mounted on slides with 7 μL of prolong gold mounting media and were visualized (60 oil-immersion objective) using a Nikon laser scanning confocal microscope , and digital images were prepared using the Nikon Imaging Elements Advanced Research Software. For the quantification of CD32-GM1 co-localization, images from at least 20 cells obtained from random fields were analyzed using the Nikon imaging software previously mentioned. Co-localization is expressed as the percentage of pixels from the CD32 channel co-localizing with pixels from the GM1 channel. For phagocytosis uptake profiles of E. coli or S. aureus covered bioparticles, monocytic cells were cultured and generated as previously explained but the protocol was adapted as follows: 1×10^4 CD14+ monocytic cells were plated in 35mM non-coated MatTek dishes (MaTek Corporation, Ashland, MA) and grown for 6 days in the absence or presence of M-CSF and/or 1, 5 or 10μM B(a)P. The cells were washed with cold PBS, and 50mg/mL of either E. coli or S. aureus covered FITC-conjugated bioparticles were added to each dish and allowed to incubate for 45 min. The rate of uptake was recorded by Nikon confocal microscope the quantification of FITC intensity of the gram positive or gram negative bioparticles in at least 20 cells selected from random fields was determined by Nikon imaging software elements advanced research.

2.12 Statistical analysis

Unless otherwise noted, results from multiple experiments are presented as ±SE. All comparisons were conducted via a one or two-way ANOVA followed by Bonferroni posthoc analysis. Values of $p \leq 0.05$ were considered to be statistically significant. When necessary, multiple comparisons of means was used to determine differences at $p<0.05$. This was accomplished by analysis of variance (ANOVA) and subsequent analysis using Tukey's honest significant difference (HSD) test at $p<0.05$.

3. RESULTS AND DISCUSSION

3.1 B(a)P exposure inhibits the differentiation of M-CSF treated blood monocytes into macrophages

To determine the effects of exposure to B(a)P on peripheral blood monocyte differentiation, monocytes were cultured with M-CSF in the presence or absence of 1μM, 5 μM and 10 μM B(a)P. As previously reported (Bournazos et al., 2009; van Grevenynghe et al., 2003) monocytes differentiated into large, adherent macrophages in the presence of M-CSF. However, upon exposure to B(a)P the differentiated monocytes displayed a large nucleus devoid of features associated with normal morphology (Fig. 3A). When cultured in the presence of 10 μM B(a)P, the number of adherent cells was markedly reduced and undifferentiated cells tended to appear smaller than those in the untreated cell cultures. A trypan blue exclusion assay (Fig. 3B) determined that exposure to B(a)P did not significantly decrease cell viability. The percentage of apoptotic cells in both unexposed monocytic cultures and B(a)P exposed monocytic cultures remained at or below 8%.

3.2 Phenotypic exposome analysis of macrophages following exposure to B(a)P

To interrogate B(a)P exposure effects on cell surface marker expression, we analyzed the levels of CD11b, CD14, CD68 and CD71 in monocytic cells cultured with M-CSF in the presence or absence of B(a)P for 6-days. First, we analyzed the levels of CD11b, a well-established macrophage marker, in untreated and B(a)P exposed cell cultures in the presence of M-CSF for 6 days (Garcia-Garcia et al., 2007; van Grevenynghe et al., 2003). Consistent with previous investigations, untreated monocytic cell cultures expressed low levels of CD11b but in the presence of M-CSF for 6 days, levels of CD11b increased 2-fold. When cultured in 10μM B(a)P for 6 days, CD11b levels returned to levels seen in untreated monocytic cell cultures (Fig. 3C). This same pattern was also seen with other surface markers including CD14 and CD71. CD14 is a monocyte surface marker usually expressed at high levels in undifferentiated cells and low levels in differentiated cells (Linch et al., 1984). The level of surface marker expression is not always consistent with previous studies as is the case with CD14 expression levels in the current study. In M-CSF treated monocytic cell cultures, CD14 levels increased. In the presence of 10μM B(a)P, however, levels returned to those seen in the untreated cell cultures. The expression levels of CD71, another well known macrophage marker, in unexposed and B(a)P exposed cells cultured in the presence or absence of M-CSF for 6 days. Following a similar pattern seen with CD11b expression, CD71 levels were low in untreated cell cultures, then increased 2-fold in cells cultured in the presence of M-CSF for 6 days, and in the presence of M-CSF and 10μM B(a)P for 6 days decreased back to levels seen in untreated monocytic cells cultures ($n = 5$, $p < 0.05$, when compared to untreated cells) (Table 1).

3.3 B(a)P exposure suppresses macrophage functional indices

An assessment of whether the effects of B(a)P exposure during M-CSF stimulation were functionally significant was undertaken. Untreated monocytic cells displayed basal levels of phagocytic ability but significantly increased when monocytic cells were cultured with M-CSF for 6 days (Fig. 4A and 4B). When cultured for 6 days in the presence of M-CSF and either 1μM, 5μM, or 10μM B(a)P, phagocytosis of FITC-dextran fluorescent microspheres was significantly suppressed when compared to the untreated cells (Fig. 4A and 4B). During the phagocytosis analysis, the cells were also incubated with CD68, a macrophage surface marker, to quantify the number of differentiated macrophages in the cell culture performing phagocytosis (Fig. 4B). As seen in Fig. 4B, there was a dose-dependent, statistically significant reduction in the expression of CD68 in monocytic cell cultures treated with M-CSF and B(a)P for 6 days.

The effects of B(a)P exposure on the respiratory burst activity of M-CSF stimulated cells and untreated cells were analyzed by exposing the cells to PMA to trigger reactive oxygen species production. Cells then were incubated with dihydrorhodamine-123, a fluorescent reactive oxygen intermediate species indicator and CD68, a macrophage surface marker. Although 1μM and 5μM B(a)P reduced phagocytosis, only 10μM B(a)P exposure was found to reduce significantly respiratory burst activity following PMA treatment when compared to the unexposed, non PMA-stimulated cells (Fig. 5A and 5B). In monocytic cells cultured in the presence of M-CSF and/or B(a)P, there was no significant difference in reactive oxygen species levels of PMA-stimulated non PMA-stimulated cells (Fig. 5B). It is important to

note that in the untreated cell cultures, there was a basal level of reactive oxygen species production.

3.4 Exposure to B(a)P suppresses uptake of gram-negative coated bioparticles

To investigate the effects of B(a)P exposure on the process of phagocytosis in S. aureus (gram-positive) and E. coli (gram-negative) bacteria, cells were cultured and prepared as previously mentioned in Materials and Methods. Briefly, 1×10^4 cells were plated in 35mm MatTek dishes, and cultured with M-CSF for 6 days in the presence or absence of 1μM, 5μM or 10μM B(a)P. Cells were harvested, washed with cold PBS, and then incubated with 1×10^8 fluorescent bioparticles/mL for 45 min. A phagocytic rate of uptake profile was generated as a recording on a Nikon confocal microscope. As seen in Fig. 6A and Fig. 6B, binding and uptake of bacteria coated bioparticles began after 10-15 min of incubation, as previously reported (Rana et al., 2014). While untreated cells exhibited a basal level phagocytosis, in cells treated with MCSF, there was a significant increase in S. aureus uptake. In cultures co-treated with M-CSF and 10μM B(a)P for 6 days, there were little to no effects on S. aureus bioparticle uptake (phagocytosis), as levels were similar to those of monocytic cells treated with only M-CSF (Fig. 6A). In contrast, co-treatment of cells with M-CSF and 10μM B(a)P suppressed the uptake of E. coli covered bioparticles (Fig. 6B).

3.5 B(a)P exposure disrupts homeostasis in macrophage membranes

After documenting the suppressive effects attributed to B(a)P exposure on M-CSF stimulated monocytic cell differentiation and functional indices, it was important to investigate potential suppression mechanisms. Other studies have also documented that CD32A (FcγRIIA) CD64 and CD16 associate with lipid rafts upon binding to IgG to initiate macrophage effector functions and that intact rafts are required for CD32-IgG binding and viral/bacterial invasion (Beekman et al., 2008; Bournazos et al., 2009; Bruhns, 2012; Olsson and Sundler, 2006; Sánchez-Mejorada and Rosales, 1998). The literature supports an argument that the effects of B(a)P exposure alter cell membrane lipid cholesterol levels and fluidity (Gorria et al., 2006; Ng et al., 1998; Tekpli et al., 2010).

To discern the ability of B(a)P exposure to impact lipid raft homeostasis and CD32-IgG complex binding, we determined the levels of IgG co-localization with lipid rafts and IgG complex binding to CD32. Monocytic cells were cultured with or without M-CSF or co-treated with M-CSF and B(a)P for 6 days. Cells were incubated with 10μg/mL hHAIgG and CD32 expression and IgG binding were assessed by flow cytometry. As can be seen in Fig. 7A, the CD32 expression and IgG binding in monocytic cell cultures stimulated with M-CSF are easily quantified. To verify previous reports that IgG binds to CD32 within lipid rafts, 1×10^4 monocytic cells were plated in 35mm MatTek dishes and cultured. Cells were stained with cholera toxin subunit B-FITC labeled (CTαB) and 10μg/mL IgG. The association of IgG with lipid rafts was determined by confocal immunofluorescence microscopy (Fig. 7B). As evident in Fig. 7B, when compared to the untreated monocytic cell cultures, 10μM B(a)P exposure reduces colocalization of IgG with the ganglioside GM1, a well-established lipid raft marker. To interrogate further IgG-CD32 binding, cells were grown as previously described and quantified by flow cytometry analysis. Again, when compared to the untreated cells, the co-treatment of M-CSF and 10μM B(a)P was found to be effective in suppressing

IgG-CD32 binding in monocytic cells (Fig. 7C). IgG-CD32 binding also was assessed after monocytic cells were cultured, harvested and treated with either 10mM MβCD (depletes membrane cholesterol) or 30μg/mL nystatin (increases membrane cholesterol). A statistically significant decrease in the IgG binding of cells treated with B(a)P, MβCD, or nystatin was observed as compared to the control (Fig.7D). It should be noted that although disruption of lipid rafts with B(a)P or MBCD had no effect on CD32 expression, we did observe an effect on CD32 distribution.

As reported by Bournazos et al. (2009), CD32 translocation to lipid rafts is associated with efficient IgG binding. They found that at rest, in the absence of IgG, CD32 resides predominantly in non-raft fractions but in the presence of 10μg/mL of hHAIgG, CD32 is redistributed to the lipid raft fractions. We investigated the effects of 10μM B(a)P exposure on this important event. Toward this end, monocytic cells were co-treated with 10μM and M-CSF, the then cells were lysed and placed in a discontinuous sucrose gradient and centrifuged for 18 h to fractionate the lipid rafts. Ten 1ml fractions were collected, the DRM fractions were determined by CD59 staining, a lipid raft marker, and analyzed for CD32 expression in the absence or presence of IgG. The fractions were also analyzed by liquid-liquid extraction and HPLC to quantify B(a)P and metabolites. As seen in Fig 8A, CD59 staining on the representative dot blot verified fractions 1-4 as non-raft fractions and fractions 6-7 as raft fractions. The dot blot was also stained against CD32 in the absence or presence of IgG. The results of the ImageJ software analysis on the dot blot indicated that in the presence of IgG, a higher percentage of CD32 is found within the lipid raft fractions as compared to the percentage of CD32 in the non-raft fractions. In the absence of IgG, there is a reduced quantity of CD32 found in raft fractions; in the presence of IgG, CD32 also is distributed at higher amounts in the non-raft fractions when compared to CD32 distribution in non-raft fraction in the presence of IgG (Fig. 8B). The 1ml fractions collected from the sucrose gradient were then analyzed for cholesterol content, B(a)P and its metabolites. A cholesterol oxidase assay measured the amount of cholesterol in each fraction and determined that fractions 5-8 contained the highest amount of cholesterol (Fig. 8C). As expected, fractions obtained from cells treated with MβCD were found to have very low levels of cholesterol. After the fractions were analyzed to verify lipid raft fractions, they were to analyzed for B(a)P metabolite content (Fig 8D) and quantified for CD32 expression and cholesterol content. The highest quantities of B(a)P and metabolites were found within the lipid raft fractions. It was interesting to note that the lipid raft fractions of cells co-treated with M-CSF and either 1, 5, or 10μM B(a)P contained the highest amount of cholesterol and B(a)P metabolites, indicating a possible relationship between B(a)P and cholesterol.

Based on the totality of the experimental evidence, we propose a mechanism for B(a)P exposure-induced suppression of macrophage effector function (Fig. 2). Suppression of macrophage effector functions occurs via disruption of lipid raft architecture to cause a decrease in CD32a within lipid rafts. As shown in Fig. 2A, we determined the cellular location of CD32a in the presence and absence of IgG, and examined the effect of B(a)P, MβCD, and nystatin on CD32a-IgG binding. Fig. 2B depicts such an interrogation of the effects of exposure to B(a)P on lipid raft cholesterol concentration and the resulting accumulation of B(a)P metabolites within lipid rafts. Our results demonstrate that in the absence of IgG, CD32a is mostly found outside lipid rafts and subsequently translocates to

lipid rafts in the presence of IgG (Fig. 2A). As indicated in Fig. 2B, the results suggest that exposure to B(a)P significantly suppresses CD32a association with lipid rafts as compared to controls, leading to reduced IgG-CD32a binding. Collectively, these findings suggest that intact lipid rafts are paramount for IgG-CD32a binding and effector function signaling, and point to a possible deleterious role for B(a)P in developmental immunotoxicological processes.

Our proposed mechanism shown in Figure 2 is in agreement with an obligatory aryl hydrocarbon receptor (AhR) mediated mechanism due to our B(a)P-exposure based experimental model system (Baba et al., 2012). The effects reported in the present report are considered to be downstream of AhR and are supported by recent studies presenting data demonstrating that the aryl hydrocarbon receptor (AhR) protects against bacterial infection by promoting macrophage survival and reactive oxygen species production. Results reported in the article by Kimura et al. (2014) support the contention that the AhR is crucial for a variety of immune responses. These authors explored the relationship between AhR and infection with the intracellular bacteria Listeria monocytogenes (LM) that admittedly is not well understood. Their data demonstrate that in response to bacterial infection, the AhR was required for clearance of the bacteria as a result of promoting macrophage survival and reactive oxygen species generation. While the results show that AhR-deficient mice were more susceptible to listeriosis, absence of the AhR receptor seemed to enhance listeriosis growth. Upregulation of pro-inflammatory cytokines was increased in AhR-deficient macrophages infected with LM despite enhanced susceptibility to LM infection. The Kimura et al. (2014) studies demonstrate that AhR protects against macrophage cell death induced by LM infection through the induction of the apoptosis inhibitor of macrophages, that promotes macrophage survival in the setting of LM infection. The data also showed that AhR promotes ROS production for bacterial clearance. In summary the Kimura et al. (2014) study demonstrates that AhR is essential to the resistance against bacterial infection by promoting macrophage survival and ROS production. In the present study and as depicted in Figure 2, AhR activation via B(a)P exposure was shown suppress macrophage functional indices and suppress uptake of gram-negative coated bioparticles.

Our mechanistic findings align with the results of a recent, 10-year retrospective cohort study that examined whether proximity to a major roadway and traffic density around the home during pregnancy was associated with risk of early life respiratory infection in a pre-birth cohort in the Boston area(Rice et al., 2015). In that study, addresses for 1,263 mother-child pairs were geo-coded subsequent to enrollment during the first trimester of pregnancy in a study known as “Project Viva” that was conducted from 1992-2002. The distance from home to nearest major roadway and traffic density were calculated within a 100 m buffer around participant's homes. Respiratory infection was defined as maternal report of at least one doctor-diagnosed pneumonia, bronchiolitis, croup, or other respiratory infection from birth until the early childhood visit (median age 3.3). A relative risk regression model was used to adjust for potential confounders and to estimate associations between traffic exposures and risk of respiratory infection. The study found that distance to roadway during pregnancy was associated with risk of respiratory infection. In fully adjusted models, relative risks (95% CI) for respiratory infection were: 1.30 (1.08, 1.55) for <100 m, 1.15 (0.93, 1.41) for 100 to <200 m, and 0.95 (0.84, 1.07) for 200 to <1,000 m compared with living ≥1,000

m away from a major roadway. Strikingly, each interquartile range increase in distance to roadway was associated with an 8% (95% CI 0.87, 0.98) lower risk, and each interquartile range increase in traffic density was associated with a 5% (95% CI 0.98, 1.13) higher risk of respiratory infection. These findings are the first to suggest that living close to a major roadway during pregnancy may predispose the developing lung to infection in early life. (Rice et al., 2015)

Similar evidence was found for the contribution of outdoor air pollution as a risk factor for tuberculosis (TB). A cross sectional study in Los Angeles hypothesized that individuals who reside near elevated pollutant exposures are likely to have a greater burden of disease – as evidenced by sputum smear-positive TB. Single factorial models yielded a significant correlation of smear-positive status and residential exposure to $PM_{2.5}$. In that study, residential distance to freeways and major arterial roads did not yield an association. This correlative report represented the first link to ambient pollution exposure as a risk factor for TB. Furthermore, $PM_{2.5}$ has the potential to impact TB lubg pathology as evidenced by the linkage of fine particulate matter levels and smear-positive TB. (Jassal et al., 2013)

4. CONCLUSION

These findings validate research trajectory 1 of the Public Health Exposome in the area of physiologic disruption (e.g. immune response) representing translational knowledge gained (on a continuum) from basic science research. Specifically, they demonstrate the critical role of exposure to traffic related air pollution (including PAHs) across gestation and an immunotoxicological molecular level mechanism that is particularly relevant during critical windows of development. They suggest that exposure to traffic related air pollution during gestation has the capacity to result in suppression of macrophage effector function by disrupting lipid raft integrity to result in reduced IgG-CD32a binding, inducing an immunosuppressive endophenotype that can lead to disparate health outcomes in vulnerable populations across the lifespan.

Since, B(a)P is the archaetypical member in the family of PAHs these data demonstrate a critical role for exposure to a key component of traffic related air pollution and its relevance to occupational exposure settings such as firefighting, coke oven, graphite electrode, and aluminum manufacturing industries, oil well and petroleum drilling operations, jet fuel handling and refuse burning etc. Our findings will also have implications for the “human toxome” studies (Bouhifd et al., 2015; Bouhifd et al., 2014). Data from our in vitro studies set a foundation upon which to build high-throughput cell-based assays that can be of fundamental use in testing the immunosuppressive potential of air-borne combustion toxicants such as PAHs. From a risk-assessment perspective, the signature responses or fingerprints for each class of immunosuppressive toxicant might be used as a repository for prioritization of chemicals to predict human toxicity.

ACKNOWLEDGMENTS

We would also like to thank Russell E. Savage, Ph.D. for critical review of the manuscript.

FUNDING INFORMATION

This study was supported, in part by R56 ES017448-01 (DBH) and S11 ES014156-05 (DBH), from the National Institute of Environmental Health Sciences. Grant R01 AA18776 (ML) jointly funded by NIAAA and NIDA. Grant NCRR RRO3032 to Meharry Medical College; 3P20MD000516-04 to PJ and DBH, and start-up funds (DBH) Division of Environmental Health Sciences, College of Public Health, The Ohio State University.

REFERENCES

Allan LL, Sherr DH. Disruption of human plasma cell differentiation by an environmental polycyclic aromatic hydrocarbon: a mechanistic immunotoxicological study. Environ Health. 2010; 9:15. [PubMed: 20334656]

Baba N, Rubio M, Kenins L, Regairaz C, Woisetschlager M, Carballido JM, et al. The aryl hydrocarbon receptor (AhR) ligand VAF347 selectively acts on monocytes and naive CD4(+) Th cells to promote the development of IL-22-secreting Th cells. Hum Immunol. 2012; 73:795–800. [PubMed: 22609446]

Beekman JM, van der Linden JA, van de Winkel JG, Leusen JH. FcgammaRI (CD64) resides constitutively in lipid rafts. Immunol Lett. 2008; 116:149–55. [PubMed: 18207250]

Bornstein MH. Sensitive periods in development: structural characteristics and causal interpretations. Psychol Bull. 1989; 105:179–97. [PubMed: 2648441]

Bouhifd M, Andersen ME, Baghdikian C, Boekelheide K, Crofton KM, Fornace AJ Jr. et al. The human toxome project. ALTEX. 2015; 32:112–24. [PubMed: 25742299]

Bouhifd M, Hogberg HT, Kleensang A, Maertens A, Zhao L, Hartung T. Mapping the human toxome by systems toxicology. Basic Clin Pharmacol Toxicol. 2014; 115:24–31. [PubMed: 24443875]

Bournazos S, Hart SP, Chamberlain LH, Glennie MJ, Dransfield I. Association of FcgammaRIIa (CD32a) with lipid rafts regulates ligand binding activity. J Immunol. 2009; 182:8026–36. [PubMed: 19494328]

Braun KM, Cornish T, Valm A, Cundiff J, Pauly JL, Fan S. Immunotoxicology of cigarette smoke condensates: suppression of macrophage responsiveness to interferon gamma. Toxicol Appl Pharmacol. 1998; 149:136–43. [PubMed: 9571981]

Bruhns P. Properties of mouse and human IgG receptors and their contribution to disease models. Blood. 2012; 119:5640–9. [PubMed: 22535666]

Claude JA, Grimm A, Savage HP, Pinkerton KE. Perinatal exposure to environmental tobacco smoke (ETS) enhances susceptibility to viral and secondary bacterial infections. Int J Environ Res Public Health. 2012; 9:3954–64. [PubMed: 23202826]

Garcia-Garcia E, Brown EJ, Rosales C. Transmembrane mutations to FcgammaRIIA alter its association with lipid rafts: implications for receptor signaling. J Immunol. 2007; 178:3048–58. [PubMed: 17312151]

Gorria M, Tekpli X, Sergent O, Huc L, Gaboriau F, Rissel M, et al. Membrane fluidity changes are associated with benzo[a]pyrene-induced apoptosis in F258 cells: protection by exogenous cholesterol. Ann N Y Acad Sci. 2006; 1090:108–12. [PubMed: 17384252]

Hart SP, Alexander KM, Dransfield I. Immune complexes bind preferentially to Fc gamma RIIA (CD32) on apoptotic neutrophils, leading to augmented phagocytosis by macrophages and release of proinflammatory cytokines. J Immunol. 2004; 172:1882–7. [PubMed: 14734773]

Jassal MS, Bakman I, Jones B. Correlation of ambient pollution levels and heavily-trafficked roadway proximity on the prevalence of smear-positive tuberculosis. Public Health. 2013; 127:268–74. [PubMed: 23453197]

Juarez PD, Matthews-Juarez P, Hood DB, Im W, Levine RS, Kilbourne BJ, et al. The public health exposome: a population-based, exposure science approach to health disparities research. Int J Environ Res Public Health. 2014; 11:12866–95. [PubMed: 25514145]

Kimura A, Abe H, Tsuruta S, Chiba S, Fujii-Kuriyama Y, Sekiya T, et al. Aryl hydrocarbon receptor protects against bacterial infection by promoting macrophage survival and reactive oxygen species production. Int Immunol. 2014; 26:209–20. [PubMed: 24343818]

Laupeze B, Amiot L, Sparfel L, Le Ferrec E, Fauchet R, Fardel O. Polycyclic aromatic hydrocarbons affect functional differentiation and maturation of human monocyte-derived dendritic cells. J Immunol. 2002; 168:2652–8. [PubMed: 11884429]

Li N, Wang M, Oberley TD, Sempf JM, Nel AE. Comparison of the pro oxidative and proinflammatory effects of organic diesel exhaust particle chemicals in bronchial epithelial cells and macrophages. J Immunol. 2002; 169:4531–41. [PubMed: 12370390]

Linch DC, Allen C, Beverley PC, Bynoe AG, Scott CS, Hogg N. Monoclonal antibodies differentiating between monocytic and nonmonocytic variants of AML. Blood. 1984; 63:566–73. [PubMed: 6365201]

Myers JN, Rekhadevi PV, Ramesh A. Comparative evaluation of different cell lysis and extraction methods for studying benzo(a)pyrene metabolism in HT-29 colon cancer cell cultures. Cell Physiol Biochem. 2011; 28:209–18. [PubMed: 21865728]

Ng D, Kokot N, Hiura T, Faris M, Saxon A, Nel A. Macrophage activation by polycyclic aromatic hydrocarbons: evidence for the involvement of stress-activated protein kinases, activator protein-1, and antioxidant response elements. J Immunol. 1998; 161:942–51. [PubMed: 9670973]

Nguyen DH, Hildreth JE. Evidence for budding of human immunodeficiency virus type 1 selectively from glycolipid-enriched membrane lipid rafts. J Virol. 2000; 74:3264–72. [PubMed: 10708443]

NIH. NIH guidelines for the laboratory use of chemical carcinogens. U.S. Dept. of Health and Human Services, Public Health Service, National Institutes of Health [Bethesda, MD]; Washington, D.C.: 1981.

Nimmerjahn F, Ravetch JV. Fcgamma receptors as regulators of immune responses. Nat Rev Immunol. 2008; 8:34–47. [PubMed: 18064051]

Olsson S, Sundler R. The role of lipid rafts in LPS-induced signaling in a macrophage cell line. Mol Immunol. 2006; 43:607–12. [PubMed: 15904959]

Popik W, Alce TM. CD4 receptor localized to non-raft membrane microdomains supports HIV-1 entry. Identification of a novel raft localization marker in CD4. J Biol Chem. 2004; 279:704–12. [PubMed: 14570906]

Ramesh, A., Archibong, A., Hood, DB., Guo, Z., Loganathan, BG. Global environmental distribution and human health effects of polycyclic aromatic hydrocarbons.. In: Loganathan, BG., Lam, PK-S., editors. Global Contamination Trends of Persistent Organic Chemicals. Taylor & Francis Publishers; Boca Raton, Florida: 2011. p. 95-124.

Rana T, Hasan RJ, Nowicki S, Venkatarajan MS, Singh R, Urvil PT, et al. Complement protective epitopes and CD55-microtubule complexes facilitate the invasion and intracellular persistence of uropathogenic Escherichia coli. J Infect Dis. 2014; 209:1066–76. [PubMed: 24259524]

Ravetch JV, Bolland S. IgG Fc receptors. Annu Rev Immunol. 2001; 19:275–90. [PubMed: 11244038]

Rice MB, Rifas-Shiman SL, Oken E, Gillman MW, Ljungman PL, Litonjua AA, et al. Exposure to traffic and early life respiratory infection: A cohort study. Pediatric Pulmonology. 2015; 50:252–259.

Sánchez-Mejorada G, Rosales C. Signal transduction by immunoglobulin Fc receptors. Journal of Leukocyte Biology. 1998; 63:521–33. [PubMed: 9581795]

Sarkar S, Song Y, Kipen HM, Laumbach RJ, Zhang J, Strickland PA, et al. Suppression of the NF-kappaB pathway by diesel exhaust particles impairs human antimycobacterial immunity. J Immunol. 2012; 188:2778–93. [PubMed: 22345648]

Simons K, Toomre D. Lipid rafts and signal transduction. Nat Rev Mol Cell Biol. 2000; 1:31–9. [PubMed: 11413487]

Stevens EA, Mezrich JD, Bradfield CA. The aryl hydrocarbon receptor: a perspective on potential roles in the immune system. Immunology. 2009; 127:299–311. [PubMed: 19538249]

Tekpli X, Rissel M, Huc L, Catheline D, Sergent O, Rioux V, et al. Membrane remodeling, an early event in benzo[a]pyrene-induced apoptosis. Toxicol Appl Pharmacol. 2010; 243:68–76. [PubMed: 19931295]

Thurmond TS, Gasiewicz TA. A single dose of 2,3,7,8-tetrachlorodibenzo-p-dioxin produces a time- and dose-dependent alteration in the murine bone marrow B-lymphocyte maturation profile. Toxicol Sci. 2000; 58:88–95. [PubMed: 11053544]

van Grevenynghe J, Bernard M, Langouet S, Le Berre C, Fest T, Fardel O. Human CD34-positive hematopoietic stem cells constitute targets for carcinogenic polycyclic aromatic hydrocarbons. J Pharmacol Exp Ther. 2005; 314:693–702. [PubMed: 15860575]

van Grevenynghe J, Rion S, Le Ferrec E, Le Vee M, Amiot L, Fauchet R, et al. Polycyclic aromatic hydrocarbons inhibit differentiation of human monocytes into macrophages. J Immunol. 2003; 170:2374–81. [PubMed: 12594260]

von Bertalanffy, L. General System Theory: Foundations, Development, Applications. G. Braziller; New York, NY, USA.: 2003.

Highlights

- The exposome provides a framework for understanding uncharacterized molecular mechanisms
- The goal was to elucidate the mechanism(s) of suppression of macrophage function.
- Exposure alters lipid raft integrity, decreases cholesterol and increases non-raft CD32
- Suggests exposures across the lifespan might induce immunosuppressive endo-phenotypes

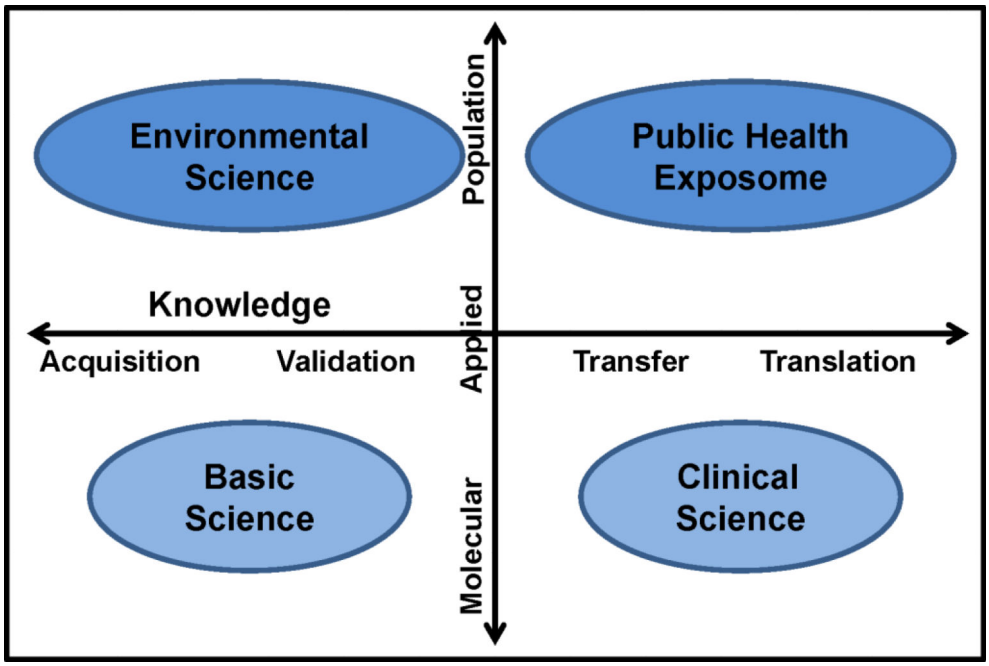

Figure 1.
Application of the public health exposome in environmental health research

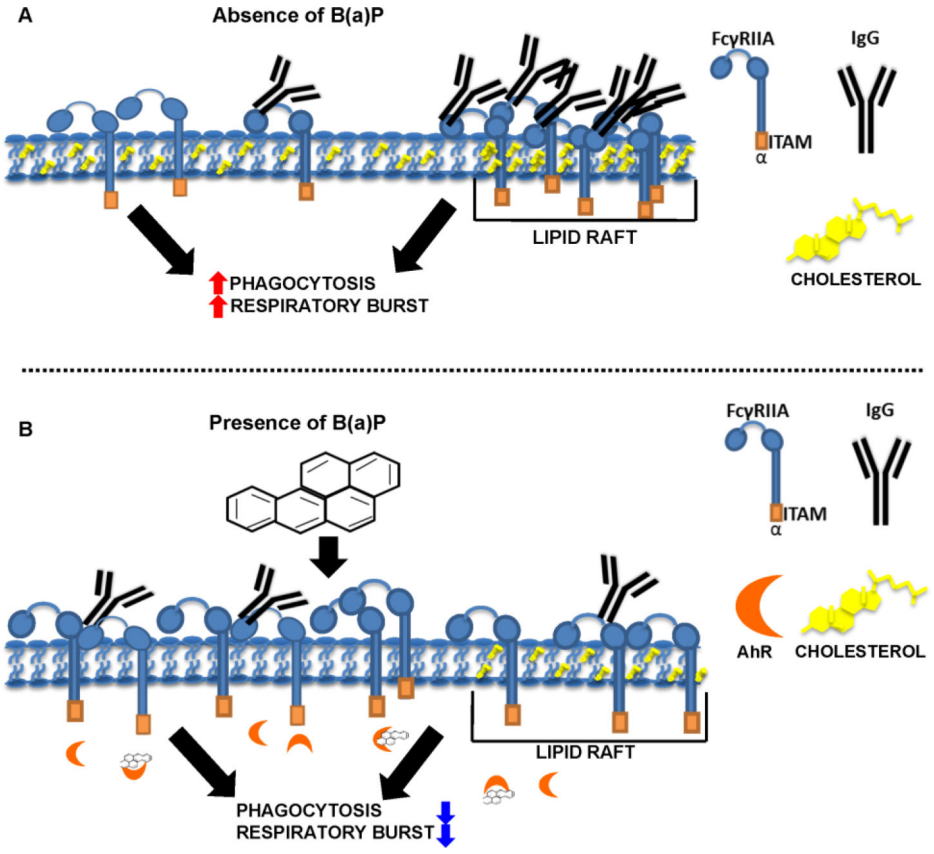

Figure 2.

Proposed mechanism for B(a)P exposure-induced suppression of macrophage effector function. Suppression of macrophage effector functions (Panel B) occurs via disruption of lipid raft architecture to cause an effective decrease in CD32a (FCγRII) within lipid rafts. We determined the cellular location of CD32a in the presence and absence of IgG, and examined the effect of B(a)P, MβCD, and nystatin on CD32a-IgG binding. Fig. 2B versus Fig 2A depicts such an interrogation of the effects of exposure to B(a)P to deplete lipid raft cholesterol concentration and the resulting accumulation of B(a)P metabolites (see Figure 8D) within lipid rafts. As is shown in Fig 2B the results demonstrate that in the absence of IgG, CD32a is mostly found outside lipid rafts and subsequently translocates to lipid rafts when in the presence of IgG (Fig. 2A). As indicated in Fig. 2B, the results suggest that exposure to B(a)P significantly suppresses CD32a association with lipid rafts as compared to controls, leading to reduced IgG-CD32a binding. Collectively our findings suggest that intact lipid rafts are paramount for IgG-CD32a binding and effector function signaling.

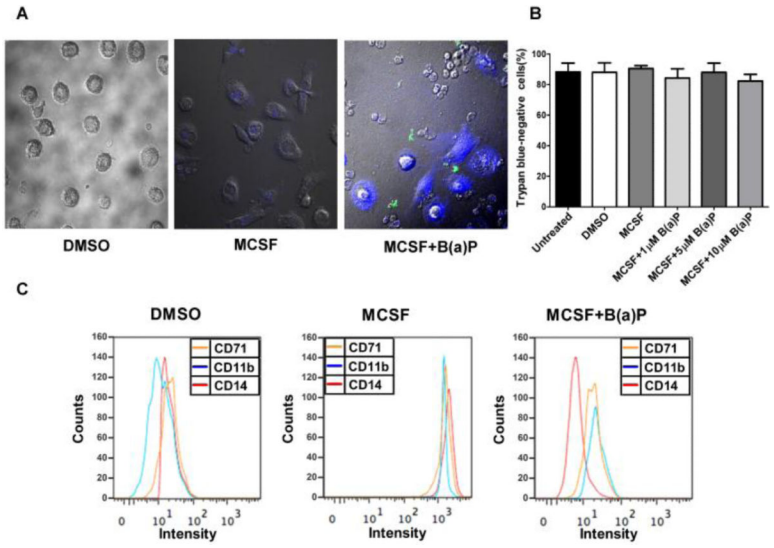

Figure 3.

B(a)P exposure inhibits the differentiation of MCSF stimulated blood monocytes into macrophages. (A) Purified human blood monocytes were cultured with MCSF in the absence or presence of 10 μM B(a)P for 6 days. Images of the cells were taken by confocal scanning laser microscopy. (B) Cell viability was assessed by trypan blue exclusion assay. (C) The cultured monocytic cells were then stained with mAbs against CD11b, CD14 or CD71. Controls were DMSO (0.01%) treated. The cells were analyzed by flow cytometry and the representative histograms from three individual experiments are as shown.

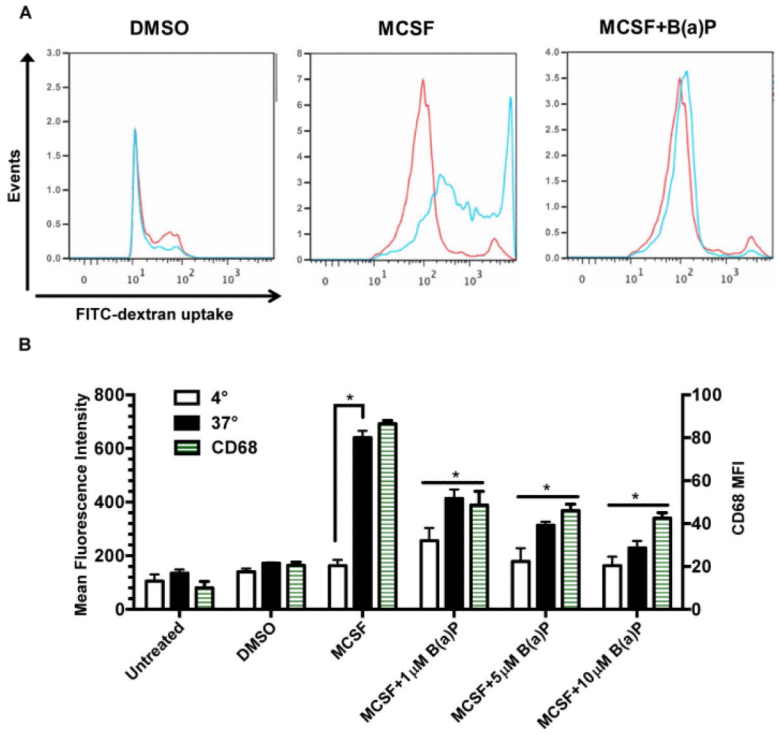

Figure 4.

B(a)P exposure decreases macrophage phagocytic activity. (A) Representative flow cytometry histograms from phagocytosis of fluorescent latex microspheres (1mg/mL) by purified human blood monocytic cells treated in the absence or presence of MCSF and 10 μM B(a)P for 6 days. Monocytic cells were incubated at 4°C or 37°C for 45 min with fluorescent latex microspheres and phagocytosis was quantified by flow cytometry. Monocytic cells incubated with microspheres at 37°C were also incubated with CD68, a macrophage marker, and quantified by flow cytometry. (B) Quantification of phagocytic activity at 4°C and 37°C. Results presented are values ± SE from at least five independent experiments. (*, $p < 0.05$) compared to DMSO-treated cells.

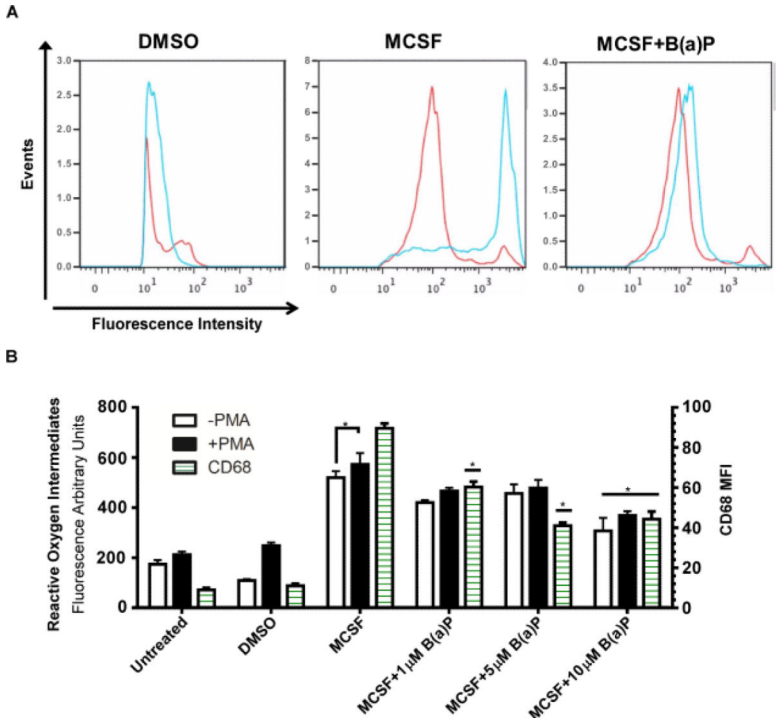

Figure 5.

B(a)P exposure decreases macrophage respiratory burst activity. (A) Representative flow cytometry histograms for PMA-stimulated respiratory burst activity in monocytic cells cultured in the absence or presence of M-CSF and/or 10μM B(a)P for 6 days. Cells were pre-stimulated with PMA for 45 min, then incubated with dihydrorhodamine 123 for 45 min. (B) The quantification of reactive oxygen species intermediate production and cells expressing CD68 when cultured in the absence or presence of M-CSF, 1, 5 or 10μM B(a)P and stimulated with or without PMA. Results presented are ± SE from at least five independent experiments. (*, $p < 0.05$) compared to untreated cells.

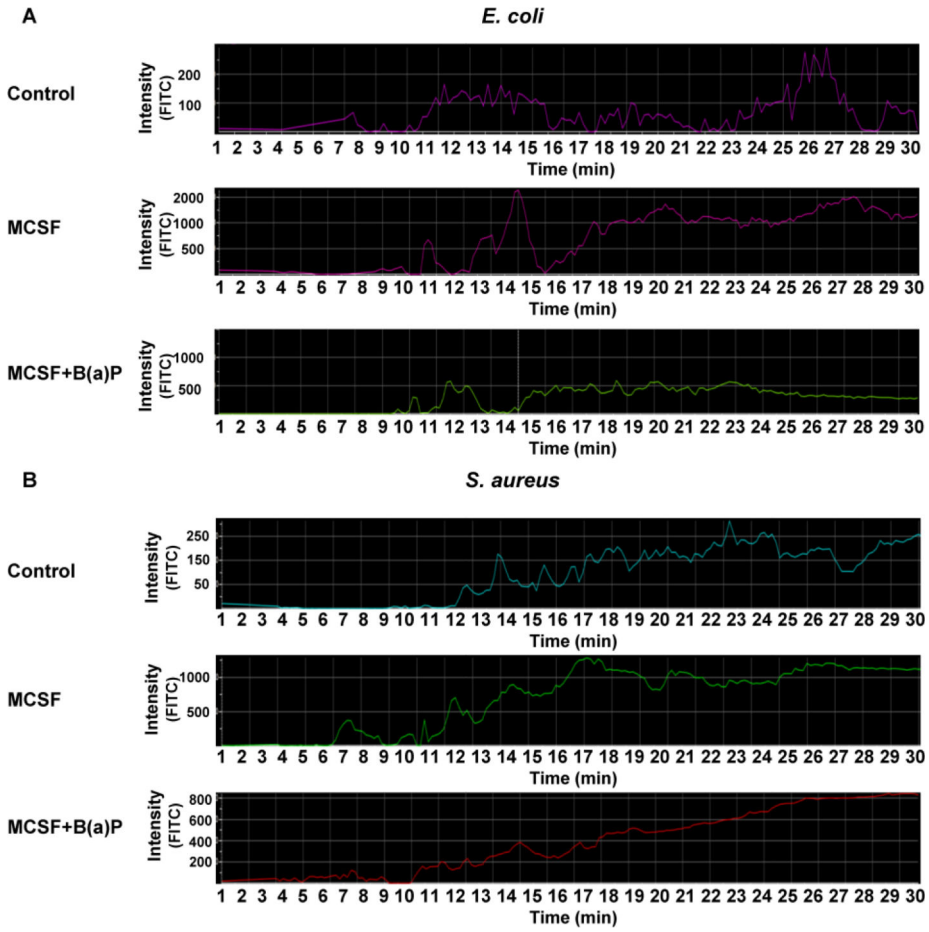

Figure 6.

B(a)P exposure suppresses uptake of E. coli bioparticles. (A) and (B) Representative confocal histogram uptake profiles for blood monocytes plated on 35mm MatTek dishes, and cultured with MCSF in the absence or presence of B(a)P (10 μM for 6 days). Cells were incubated with E. coli or S. aureus FITC-conjugated bioparticles (50 mg/mL for 45 min) and phagocytic rate of uptake profiles were recorded by confocal microscope. Twenty cells were selected and the uptake profile for each was analyzed. (A) Representative uptake profiles from E. coli covered bioparticles and (B) S. aureus covered bioparticles. Results presented are values ± SE from at least five independent experiments. (*, $p < 0.05$) compared to DMSO-treated cells.

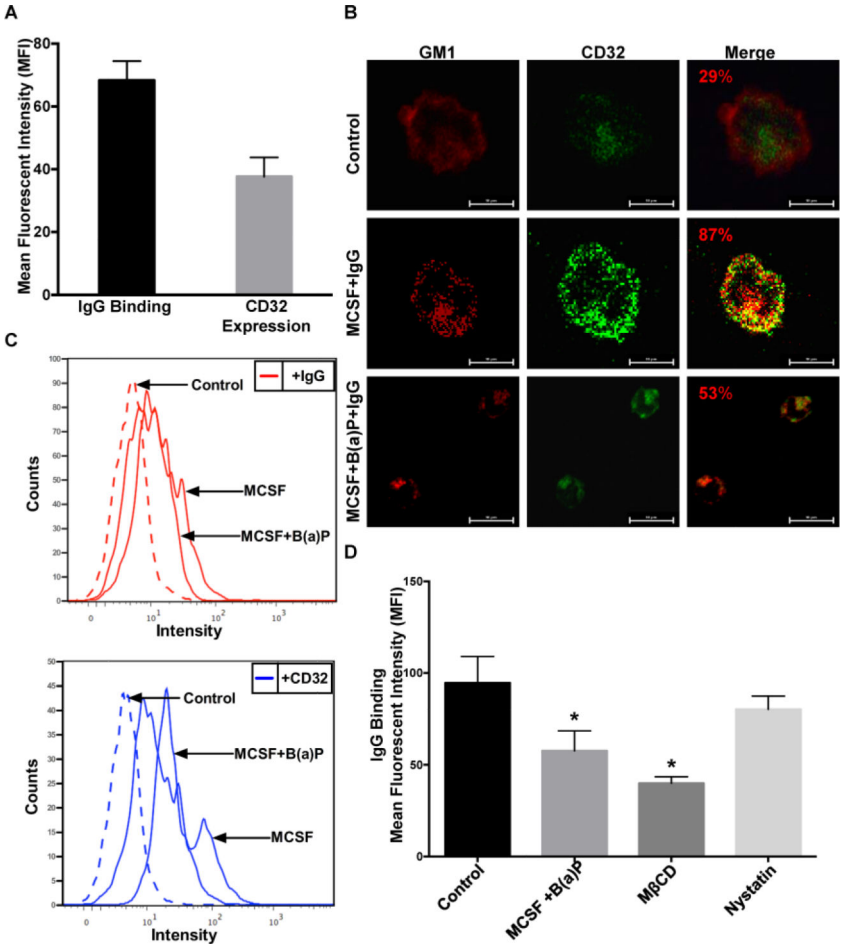

Figure 7.

B(a)P exposure disrupts lipid raft homeostasis. (A) Quantification of IgG complex binding to CD32 in untreated $CD14^{+}$ monocytic cells. Cells were incubated with human heat aggregated IgG (hHAIgG-10μg/mL) for 30 min, then stained for CD32a. (B) Representative confocal immunofluorescence micrographs of monocytic cells treated with IgG (hHAIgG-10μg/mL) for 30 min, stained for ganglioside 1 (GM1-a marker for lipid raft domains) with CTαB-AF555 (Red) and for CD32-PE (Green) mean fluorescent intensity was determined by nikon imaging software. Cells were prepared and analyzed as described in Materials and Methods. (C) Representative flow cytometry histograms of IgG and CD32 expression in monocytic cells exposed to MCSF or MCSF+B(a)P. The cells were incubated with hHAIgG-FITC conjugated (10μg/mL) for 30 mins, then stained for CD32-PE. (D) Measurement of IgG complex binding to CD32 in monocytic cells exposed to either B(a)P (10μM), MβCD (10 mM 15 min at 37°C), or nystatin (30μg/mL for 15 min at 37°C). Results presented the mean (±SE) from at least three independent experiments (*, $p < 0.05$) compared with untreated control cells.

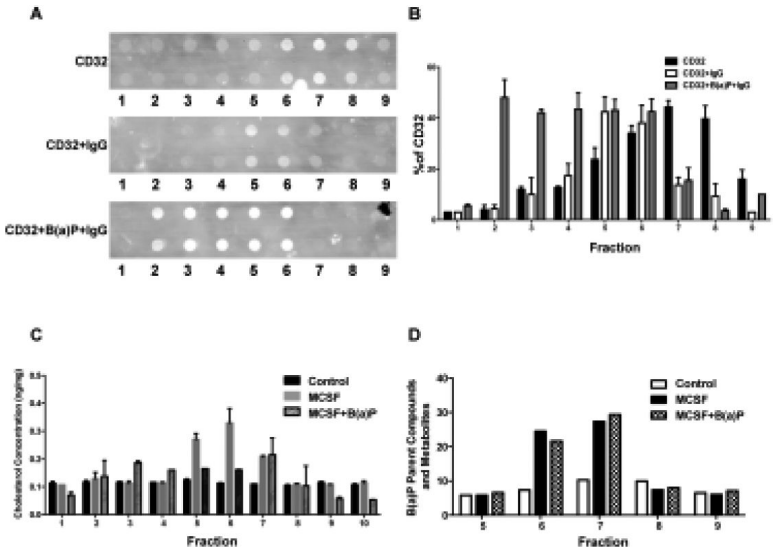

Figure 8.

B(a)P exposure results in decreased IgG-CD32 binding within lipid raft regions. Cells were prepared and analyzed as described in Methods. (A) DRM fractionation and analysis of CD32 distribution in monocytic cells treated with M-CSF and 10 μM B(a)P for 6 days. Following treatment of cells with 10 g/mL hHAIgG to determine receptor localization following IgG complex binding. CD59 was used as a marker for DRM fractions. (B) Quantification of CD32 band intensities present in each fraction (Image J software). (C) After cells were cultured and fractionated as described in Methods, the subsequent 1 mL fractions were analyzed for cholesterol content by cholesterol oxidase assay. (D) In parallel, the 1 mL fractions were analyzed by liquid-liquid extraction and HPLC analysis to measure B(a)P metabolite concentration.

Table 1

Phenotypic analysis of human blood monocytic cells cultured in the absence or presence of B(a)P

Surface Marker	DMSO	B(a)P (10 μM)
CD11b (n=7)	451.4 ± 162.6	394.8 ± 229.5
CD14 (n=7)	13.7 ± 3.3	12.1 ± 5.4
CD68 (n=7)	213.7 ± 96.2	151 ± 76.5
CD71 (n=7)	86.2 ± 55.4	10.5 ± 16
CD86 (n=7)	84.2 ± 10.1	121.9 ± 8.1